

Article

The Kinetic Mechanism of the Thermal Decomposition Reaction of Small Particles of Limestone at Steelmaking Temperatures

Chenxiao Li ¹, Yun Zhang ¹, Yuekai Xue ^{1,*}, Kaixuan Zhang ¹, Shuhuan Wang ¹, Huakang Sun ¹ and Huaqing Xie ^{2,*}¹ Metallurgy and Energy College, North China University of Science and Technology, Tangshan 063210, China² School of Metallurgy, Northeastern University, Shenyang 110819, China

* Correspondence: xueyuekai965@163.com (Y.X.); huaqing_2008@163.com (H.X.); Tel.: +86-150-3159-5965 (Y.X.); +86-024-8367-2216 (H.X.)

Abstract: Converter blowing limestone powder making slag steelmaking process has the advantages of low carbon and high efficiency, and can realize the resource utilization of CO₂ in the metallurgical process, which is in line with the development direction of green metallurgy. Based on a thermogravimetric-differential thermal analyzer, the kinetic mechanism of decomposition of small limestone at steelmaking temperatures was investigated by a modified double extrapolation method. The results showed that with a higher rate of heating, limestone decomposition lagged, and decomposition temperature increased. Furthermore, the smaller the limestone particle size, the lower the activation energy of decomposition. Compared with N₂, air, and O₂, small limestone powder used for converter blowing could complete more rapid decomposition, and the time required for decomposition shortened by about 1/3, although the decomposition temperature increased in the CO₂. The limestone decomposition rate increased and then decreased at low to high CO₂ partial pressures. With a limiting link, the inhibition was more significant under high CO₂ partial pressure, but the reaction can be fully completed by 1000 °C. The decomposition type modeled was stochastic nucleation and subsequent growth. As the partial pressure of CO₂ increased from 25% to 100%, the number of reaction stages, *n*, increased.



Citation: Li, C.; Zhang, Y.; Xue, Y.; Zhang, K.; Wang, S.; Sun, H.; Xie, H. The Kinetic Mechanism of the Thermal Decomposition Reaction of Small Particles of Limestone at Steelmaking Temperatures. *Processes* **2023**, *11*, 2712. <https://doi.org/10.3390/pr11092712>

Academic Editor: Carlos Sierra Fernández

Received: 28 August 2023

Revised: 8 September 2023

Accepted: 8 September 2023

Published: 11 September 2023



Copyright: © 2023 by the authors. Licensee MDPI, Basel, Switzerland. This article is an open access article distributed under the terms and conditions of the Creative Commons Attribution (CC BY) license (<https://creativecommons.org/licenses/by/4.0/>).

Keywords: converter steelmaking; small-particle limestone; decomposition kinetics; carbon dioxide partial pressure; low carbon

1. Introduction

The steel industry, as a highly intensive, highly industrialized, and wide-ranging industry, accounts for about five percent of the gross domestic product (GDP) of China and plays an indispensable role in stimulating economic and industrial development, making it a veritable pillar industry. At the same time, the rapid development of the iron and steel industry has brought about the environmental problems of high carbon emissions and high energy consumption. At present, the iron and steel industry is mainly based on the “blast furnace–converter” process of steelmaking. In the context of the “carbon neutrality and carbon peak” era, the development of the iron and steel industry is bound to gradually transform to low carbon and green. As an important part of the process, the converter steelmaking process is facing the serious challenge of carbon reduction and energy saving to realize deep carbon reduction [1–3]. Converter smelting links mostly use lime slag for steelmaking, but the production and transportation of lime for steelmaking produces a lot of pollution. In the process of converter application due to the low activity of lime, the dephosphorization rate is generally around 40–60% [4]. Part of the input of large pieces of lime is to a certain extent caused by slag difficulties [5–8], but the subsequent smelting also has a certain impact. The main component of limestone is CaCO₃, which is decomposed into CaO and CO₂ at high temperatures. CaO can be used as slagging material in the

converter process, and the released CO₂ can participate in the melting pool reaction. For this reason, limestone is added into the converter as a slagging material. At the same time, the task of slag making and dephosphorization is accomplished; however, this can also be accomplished through the resource utilization of CO₂, which greatly reduces the cost of CO₂ emissions. Li et al. [9] proposed a converter limestone technique instead of lime-slagging steelmaking, capitalizing on the use of converter steelmaking conditions to achieve the production and application of high-activity lime. Compared with the traditional slagging steelmaking process, the use of limestone instead of lime-slagging steelmaking in converter steelmaking to meet the needs of smelting is based on an effective increase in the rate of dephosphorization. The dephosphorization process is also more stable and material consumption is reduced. Moreover, the CO₂ generated from the decomposition of limestone in the converter can react with the elements in the hot liquid iron to generate CO, which increases the amount of gas recovery and the concentration of CO [10–13]. Mao et al. confirmed through industrial tests that the slagging of limestone in the converter can lead to the volatilization of some silicon elements in the hot liquid iron, thus reducing the amount of slag [14–16]. Moreover, during the decomposition of limestone in the converter, the CO₂ produced can not only be used as part of the endogenous oxygen source to replace oxygen in the steelmaking reaction, but the escape of CO₂ can also lead to the improvement of the molten pool kinetic conditions [17–19]. However, while limestone shows certain advantages in rapid slagging and phosphorus removal, limestone particle size also affects melting in the converter; Deng et al. [20] found that the decomposition of the surface layer of massive limestone at steelmaking temperatures produces a dense structure of lime and affects the further decomposition of limestone. Lu et al. [21] found that the addition of large blocks of limestone is not conducive to the improvement of phosphorus removal efficiency. Therefore, the study of the decomposition degree and decomposition mechanism of limestone at steelmaking temperatures is one of the hot spots in the study of slagging steelmaking by replacing lime with converter limestone. Liang et al. [22], through a thermal state experimental study, found that limestone replacement of lime for slagging steelmaking is practicable. A limestone substitution ratio of 40% to 60% has a significant impact on the effect of dephosphorization, and the limestone particle size should not be too large to ensure that it can be quickly decomposed. Tang et al. [23], through the corresponding physical simulation, found that the powder penetration ratio increases with an increase in powder particle size. Furthermore, limestone particles in the spray travel through the gas–liquid interface into the melt pool when there is a critical diameter. Zhang et al. [24], through the use of a spray gun water simulation test, found that the limestone particle size is one of the main influencing factors affecting the powder blowing speed; a change in the blowing speed will thus have a chain of effects on the blowing effect. Too large a blowing particle size will lead to an increase in the blowing resistance, dispersing part of particles and making it so the particles cannot pass through the gas–liquid interface into the molten pool. Wang et al. [25] studied the decomposition mechanism of 4–25 mm limestone at high temperatures and found that the reaction of large-size limestone follows the model of random nucleation and subsequent growth, and the number of reaction stages was 3/4; Cao et al. [26] used a differential thermal analyzer to study the reaction mechanism of the high-temperature calcination of limestone under an air atmosphere of air and a mixed air–carbon dioxide atmosphere and found that different reaction atmospheres change the model of limestone decomposition, and the decomposition temperature and activation of the decomposition of limestone under the mixed atmosphere are also changed. The limestone decomposition temperature and decomposition activation energy are higher than in a pure air atmosphere. Zhang et al. [27] used a double extrapolation method to study the kinetic parameters of the limestone thermal decomposition reaction under a high concentration of carbon dioxide and found that the reaction follows the stochastic nucleation and stochastic growth model, and the number of reaction stages, *n*, is different under different carbon dioxide concentrations. Chen et al. [28] studied the decomposition mechanism of limestone with a particle size of 10 mm or less through thermogravimetric

experiments and found that the higher the temperature and the smaller the particle size, the faster the decomposition rate of limestone, and that the particle size and the calcination temperature also have a significant effect on the thermal decomposition mechanism of limestone. Several studies have been conducted to confirm the advantages of converter limestone slagging for phosphorus removal; however, the limestone decomposition process consumes a large amount of heat, especially when large quantities are added centrally from the top through the silo. In addition, the additional limestone diameter is generally between 10 and 40 mm. A larger limestone block is not easy to calcine, and if the limestone and the initial slag contact to form a harder slag shell, the reaction surface activity is reduced, which is not conducive to the subsequent slag process, resulting in CO₂ that is not utilized. Furthermore, the density of limestone is about 2.7 g/cm³; after directly added it through the top of the converter, even with the stirring effect of top-blowing oxygen, part of the limestone will float in the upper part of the molten pool, and the CO₂ generated by the decomposition of limestone cannot fully contact the molten pool, so the CO₂ utilization rate is not high.

Li et al. [29,30] proposed the use of converter-blown limestone powder slag steel-making, in which carrier gas is used to blow small-particle-size limestone into the molten pool. The study found that to avoid the defects caused by block limestone, and at the same time give full play to the advantages of limestone in the slag steelmaking link, the slag dephosphorization conditions and the efficiency of the reaction need to be improved. Sun et al. [31], in their research on the rapid calcination decomposition behavior of small particles of limestone at converter steelmaking temperatures, found that the conversion rate of the decomposition of small particles of limestone is faster and more likely to produce high activity than lime. In addition, the dephosphorization effect of an average particle size of 0.44 mm of small particles of limestone using the carrier gas jet blowing into the converter melting pool is better. Although the high temperature decomposition behavior of small particles of limestone and the converter dephosphorization effect have been the subjects of a large number of preliminary studies, at present, the kinetic mechanism of the decomposition of small particles of limestone under converter steelmaking temperatures has undergone less research. By studying the thermal decomposition behavior of small-grained limestone at the temperature of converter steelmaking, the authors clarified the kinetic parameters of the rapid calcination and decomposition of small-grained limestone at high temperatures and the reaction mechanism of converter blowing of small-grained limestone for slag-making and steelmaking functions by using the improved double extrapolation method in the hope of providing a theoretical basis for further applications.

2. Materials and Methods

2.1. Materials

The raw material used in the test was limestone for steelmaking from Shijiazhuang, and the chemical composition of the sample was determined by XRF, as shown in Table 1. After the calcination of the limestone, the mass fraction of CaO in the limestone reached 54.38% and the impurity content was low, indicating the high quality of limestone.

Table 1. Chemical composition of limestone (% wt.).

CaO	MgO	SiO ₂	SO ₃	Al ₂ O ₃	Fe ₂ O ₃	K ₂ O	Others	Loss
54.38	0.96	0.17	0.01	0.234	0.258	0.08	0.056	43.875

2.2. Methods

The raw materials used in the tests were limestone with particle sizes of 0.18–0.68 mm and 2–3 mm, with average particle sizes of 0.44 mm and 2.5 mm, respectively. Raw limestone was simply cleaned of some of the impurities present on the surface with anhydrous ethanol before being crushed and left to dry naturally. Then, the experimental raw materials were crushed by a jaw crusher, and the limestone particles with different particle size ranges

were sieved using standard sieves of different mesh sizes. The sieved limestone particles were washed with fresh water, dried in a drying oven for 48 h, and then vacuum-sealed in a sealed bag.

The temperature range of the thermogravimetric-differential thermal analyzer used in the test can reach 25–1600 °C. An alumina crucible was selected, the sample mass was weighed with a precision balance as (20 ± 0.1) mg, and the experimental atmospheres were the standard gas of nitrogen, oxygen, and carbon dioxide, standard carbon dioxide, and nitrogen mixed with carbon dioxide at carbon dioxide partial pressures of 0%, 25%, 50%, 75%, and 100%, respectively. The gas flow rate was set to 20 ML/min, and the sample was heated from 25 °C to 1100 °C after setting the heating rate so that the limestone was completely transformed to a stable state and the complete thermal decomposition curve of limestone was obtained.

2.3. Calculation Methodology

The conversion rate, α , of the limestone samples was calculated from Equation (1) through the weight loss of limestone.

$$\alpha = \frac{w_0 - w_t}{w_0 - w_x} \times 100\% \quad (1)$$

where α is the conversion rate of the limestone, w_0 is the original weight of the limestone sample, w_t is the weight of the limestone sample at a point t of the reaction, and w_x is the mass of the sample at the complete decomposition.

In performing the computational solution of the kinetic parameters and the most probabilistic mechanism function, the double extrapolation method combining the Flynn–Wall–Owaza method and the Coats–Redfern method is often applied nowadays [32]. In this paper, we adopt the improved double extrapolation method, using the combination of the Starink differential and the Coats–Redfern integral with higher precision, mainly because the Starink differential equation makes a detailed categorization and comparison for the Flynn–Wall–Owaza method. The partial integral and Doyle’s approximation of the temperature integral are analyzed, and the temperature integral term is rationally corrected by linear regression. Thus, it will fit more accurately and achieve a smaller relative error in $E_{\alpha \rightarrow 0}$. We fix the conversion rate, α , and extrapolate α to 0 by fitting to obtain the value of $E_{\alpha \rightarrow 0}$ without any interference of side reactions and assuming the system is in the pristine state, i.e., the activation energy of the nucleation of the new phases. Furthermore, we fix the rate of heating, β , and obtain the kinetic parameter $E_{\beta \rightarrow 0}$ when β is extrapolated to 0 by fitting to clarify the most probable mechanism function of limestone decomposition.

The kinetic equation for the gas–solid chemical reaction is:

$$\frac{d\alpha}{dt} = kf(\alpha) \quad (2)$$

where k is the reaction rate constant, t is the reaction time, and $f(\alpha)$ is the reaction mechanism function in differential form.

The reaction rate constant k versus the thermodynamic temperature T was obtained according to the Arrhenius formula for a non-isothermal, non-homogeneous system:

$$k = Ae^{-E/RT} \quad (3)$$

where E is the activation energy, A is the finger forward factor, and R is the gas reaction constant, 8.3145 J/mol·K.

The kinetic equation for the non-isothermal non-homogeneous phase is thus obtained:

$$\frac{d\alpha}{dT} = \frac{A}{\beta} e^{-E/RT} f(\alpha) \quad (4)$$

where β is the heating rate.

The kinetic model function in integral form is obtained:

$$G(\alpha) = \int_{T_0}^T \frac{A}{\beta} e^{-E/RT} dT = \frac{A}{\beta} \int_{T_0}^T e^{-E/RT} dT = (AE/\beta R)P(u) \quad (5)$$

where $P(u)$ is the temperature integral, $P(u) = \int_{\infty}^u -(e^{-u}/u^2)du$, $u = E/RT$ and T_0 is the initial reaction temperature.

The Starink differential [19] is:

$$\ln(\beta/T^{1.8}) = C_s - 1.0037E/RT \quad (6)$$

where C_s is the univariate function of $G(\alpha)$ when the conversion rate α is fixed, $G(\alpha)$ is fixed, and C_s is constant.

We fixed $\ln(\beta/T^{1.8})$ as the Y-axis and $1/T$ as the X-axis, and made a linear fit to a straight-line graph according to $Y = AX + B$. According to the slope of the fitted straight line, the apparent activation energy corresponding to a fixed conversion rate α was obtained. Using Equation (7), α was extrapolated to zero, and the value of $E_{\alpha \rightarrow 0}$ was obtained, which was the value of $E_{\alpha \rightarrow 0}$ without any interference of side reactions when the system was in the original state.

$$E = \alpha_1 + b_1\alpha + c_1\alpha^2 + d_1\alpha^3 \quad (7)$$

The Coats–Redfern integral is written as:

$$\ln(G(\alpha)/T^2) = \ln(AR/(\beta E)) - E/(RT) \quad (8)$$

We fixed $\ln(G(\alpha)/T^2)$ as the Y-axis and $1/T$ as the X-axis, according to $Y = AX + B$ for a linear-fitting straight-line graph, analyzing the slope of the fitted straight line to find the apparent activation energy, E , corresponding to a fixed rate of temperature increase, β . The closer the linear correlation coefficient R^2 is to 1, the higher the degree of fit, and the more the functional form of $G(\alpha)$ represents the real situation of the reaction process. Then, 47 commonly used kinetic mechanism functions [32] were utilized, from which the $G(\alpha)$ equation with high linear correlation and kinetic parameters in line with the general law of thermal decomposition reaction was selected, and the corresponding kinetic parameters were calculated from it. Using Equation (9) to extrapolate β to zero, the kinetic parameters of the sample in the thermal equilibrium state and the value of $E_{\beta \rightarrow 0}$ were obtained.

$$E = \alpha_2 + b_2\beta + c_2\beta^2 + d_2\beta^3 \quad (9)$$

When comparing the two extrapolated $E_{\alpha \rightarrow 0}$ values with the $E_{\beta \rightarrow 0}$ values, if they are equal or similar, the corresponding $G(\alpha)$ mechanism function equation can be considered the most probable mechanism function in the thermal decomposition process of limestone.

3. Results

3.1. Effect of Particle Size on the Thermal Decomposition Reaction of Small-Particle Limestone

To study the effect of particle size on the decomposition kinetics of limestone under rapid heating conditions, we selected the average particle sizes of 0.44 mm limestone and 2.5 mm (the maximum particle size allowed in the test) limestone as comparison points to observe their decomposition performance. Combined with the converter-blowing limestone-powder slagging steelmaking technology, taking into account 1 mol of carrier gas carrying 1 mol of limestone powder into the molten pool inside, and 1 mol CaCO_3 in the thermal decomposition of 1 mol CO_2 , we selected a decomposition furnace atmosphere of 50% CO_2 /50% N_2 for the test. We selected the heating rate to simulate the temperature environment of the converter as far as possible and combined it with the actual operation of the thermogravimetric-thermal equipment. Figure 1 below shows the thermal decomposition curves of 0.44 mm limestone.

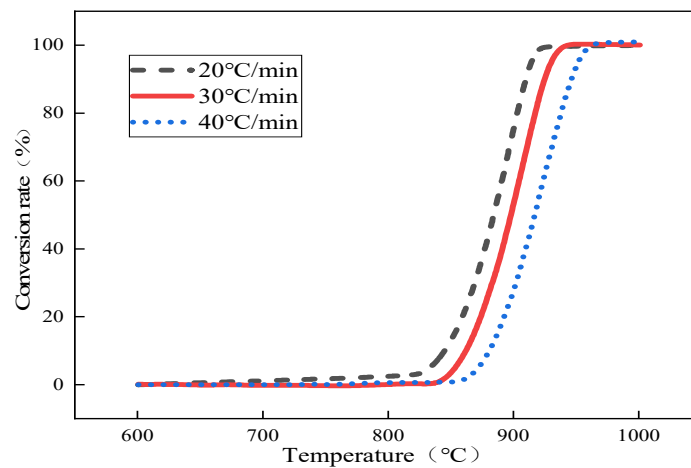


Figure 1. The conversion rate curve of 0.44 mm small particles of limestone with temperature changes.

The thermal decomposition of limestone with an average particle size of 0.44 mm was analyzed as an example, and the corresponding temperatures of the conversion rates of limestone at different heating rates were obtained according to the conversion rate curves of limestone, as shown in Table 2 below. The conversion rate was fixed first, and according to the Starink differential equation $\ln(\beta/T^{1.8}) = C_s - 1.0037E/RT$, the inverse $1/T$ of the values of small limestone particles at different heating rates and corresponding reaction temperatures were substituted, the linear fitting relationships between $\ln(\beta/T^{1.8})$ and $1/T$, and the corresponding fitting coefficients R^2 according to the slope of the linear equations obtained by fitting the activation energy E under the corresponding conversion rate are shown in Table 3 below. Then, according to Equation (7), α was extrapolated to 0, and the activation energy $E_{\alpha \rightarrow 0} = 250.32 \text{ kJ} \cdot \text{mol}^{-1}$ was obtained without any interference from side reactions when the system was in the original state; the fitting results are shown in Figure 2.

Table 2. Reaction temperatures for each conversion rate at different heating rates.

Conversion Rate (%)	Temperature/°C (20 °C/min)	Temperature/°C (30 °C/min)	Temperature/°C (40 °C/min)
20	863.37	878.9	892.51
30	870.91	886.93	901.13
40	878.8	895.12	909.64
50	886.5	902.22	917.12
60	890.66	908.29	923.82
70	896.87	915	931.06
80	902.88	921.46	937.77
90	909.59	929.98	946.35

Table 3. Corresponding linear fitting equations for different conversion rates in 50%CO₂.

Conversion Rate (%)	Linear Fitting Equation	Fitting Factor (R^2)	E (kJ·mol ⁻¹)
20	$\ln(\beta/T^{1.8}) = -29516 \frac{1}{T} + 16.312$	0.9968	244.51
30	$\ln(\beta/T^{1.8}) = -28801 \frac{1}{T} + 15.504$	0.9965	238.58
40	$\ln(\beta/T^{1.8}) = -28594 \frac{1}{T} + 15.14$	0.9963	236.87
50	$\ln(\beta/T^{1.8}) = -28189 \frac{1}{T} + 14.636$	0.9962	233.51
60	$\ln(\beta/T^{1.8}) = -27064 \frac{1}{T} + 13.554$	0.9967	224.19
70	$\ln(\beta/T^{1.8}) = -26496 \frac{1}{T} + 12.935$	0.9965	219.49
80	$\ln(\beta/T^{1.8}) = -26212 \frac{1}{T} + 12.568$	0.9968	217.14
90	$\ln(\beta/T^{1.8}) = -25087 \frac{1}{T} + 11.475$	0.9992	207.82

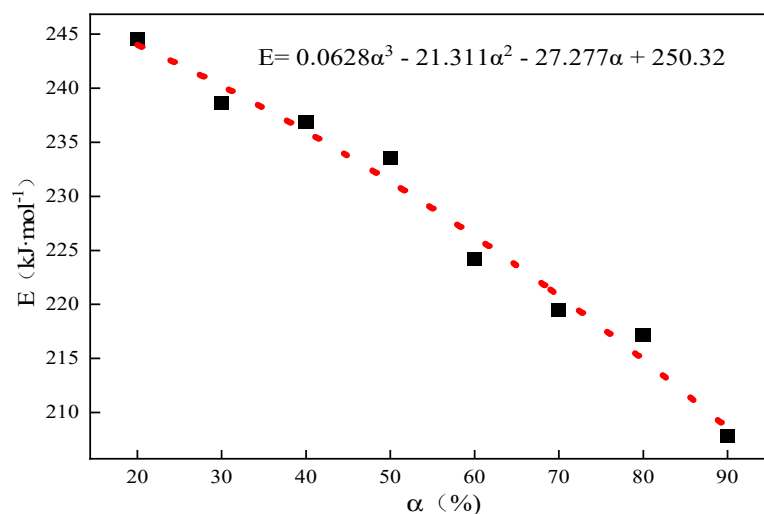


Figure 2. The curve of activation energy E to α for the thermal decomposition of 0.44 mm limestone.

Similarly, we analyzed the kinetic parameters of limestone with an average particle size of 2.5 mm for extrapolation. The apparent activation energy of the limestone decomposition was $328.27 \text{ kJ}\cdot\text{mol}^{-1}$; with the increase in limestone particle size, the apparent activation energy of limestone thermal decomposition increases and the decomposition reaction difficulty increases. The particle size of limestone used in steelmaking is 10–40 mm, which is much larger than that of the limestone selected in the test; therefore, with the further increase in particle size, the activation energy of decomposition will increase more and more, and the difficulty of decomposition will be greater. The decomposition of small-grained limestone will be better under the environment of steelmaking in the converter to provide better conditions for slag dephosphorization.

3.2. Effect of Atmosphere on the Thermal Decomposition Reaction of Small-Particle Limestone

Converter-blowing limestone steelmaking technology uses a carrier gas to carry small particles of limestone to the molten iron pool, where the heat transfer process is no longer restricted and the limestone can be rapidly heated for decomposition and calcination to generate a large surface area with large porosity, small pile density, and the high activity of high-quality lime. Furthermore, the slagging effect and dephosphorization rate are improved, and the CO_2 released in the decomposition acts as a source of endogenous oxygen to participate in the steelmaking reaction, improving the dynamic conditions of CO_2 resource utilization. Therefore, this subsection investigates the thermal decomposition behavior of small-grained limestone in different decomposition furnace atmospheres. To make the heat of the small-particle limestone more uniform when studying the effect of the thermal decomposition of small-particle limestone under different decomposition atmospheres, the selected heating rate was $10 \text{ }^\circ\text{C}/\text{min}$, and the average particle size of the selected limestone was 0.44 mm. The TG-DTG curves of the small-particle limestone in four reaction atmospheres, namely, N_2 , air, O_2 , and CO_2 , are shown in Figure 3.

From Figure 3a, it can be seen that in the N_2 , air, and O_2 atmospheres, the limestone decomposition onset and completion temperature were roughly equivalent; the initial decomposition temperature was close to $643 \text{ }^\circ\text{C}$, the endpoint of the decomposition temperature, when the decomposition was completed, was at about $847 \text{ }^\circ\text{C}$. The initial decomposition temperature of limestone under the pure CO_2 atmosphere was about $900 \text{ }^\circ\text{C}$, and the terminal decomposition temperature was close to $970 \text{ }^\circ\text{C}$, with a weight loss rate of about 43.5%. Small particles of limestone in all four atmospheres were fully reacted within $1000 \text{ }^\circ\text{C}$. The change in the limestone decomposition temperature under different carrier gas atmospheres was mainly because limestone produces part of the CO_2 during the decomposition process. Therefore, compared with other atmospheres, the presence of CO_2

in the pure CO₂ atmosphere significantly inhibits the limestone decomposition behavior, so that the activation energy required for decomposition is increased, the reaction is not easy to carry out, and the decomposition temperature is increased.

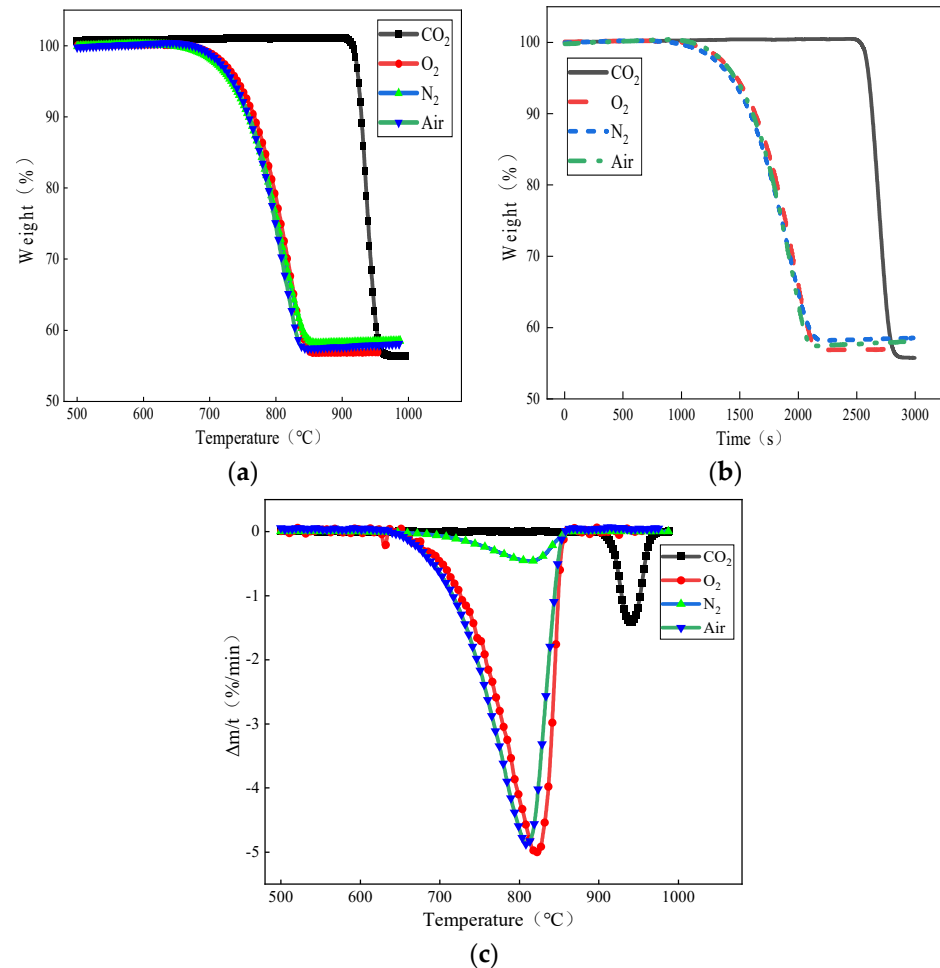


Figure 3. Effect of carrier gas atmosphere on limestone decomposition: (a) weight loss versus temperature curves under different atmospheres; (b) curves of weight loss with decomposition time under different atmospheres; and (c) DTG curves of limestone decomposition under different atmospheres.

In addition, as can be seen from Figure 3b, under the atmospheres of N₂, air, and O₂, the decomposition of limestone from the beginning to the completion of the decomposition took about 1100 s, while under the atmosphere of pure CO₂, the initial decomposition temperature of the small particles of limestone was increased, but the decomposition time required was instead shortened by about 1/3, and the decomposition was completed in about 390 s. Combined with the actual environment of the converter steelmaking, in which the converter temperature can reach more than 1350 °C and small particles of limestone in the carrier gas jet are blown into the converter pool, the heat transfer rate would be much greater than the experimental rate of heating, the limestone decomposition would be more intense and rapid, and the decomposition time would be much shorter, with the decomposition quickly completed to obtain the high activity of lime.

From Figure 3c, it can be seen that in the limestone decomposition process, there is an “S” shaped peak. In the initial reaction stage, the limestone decomposition rate is slower; in the middle, the limestone decomposition rate began to accelerate to a certain level; and the end of the reaction, the limestone decomposition rate gradually slows down until the reaction is complete. This is because with the increase in temperature, the limestone heat transfer efficiency increases, which makes the limestone decomposition faster. In addition,

compared to the other atmospheres, the peak of the DTG curve in the CO₂ atmosphere lags behind the peak weight loss rate of the other three curves, peaking at about 937 °C.

3.3. Effect of CO₂ Partial Pressure on the Thermal Decomposition Behavior of Small-Particle Limestone

To further study the effect of small-particle limestone on the reaction limit and decomposition behavior under different CO₂ partial pressures, based on the above study, experiments were carried out using an atmosphere of carbon dioxide and nitrogen mixed with standard gas and increasing the CO₂ partial pressure for three groups of experiments of 25%, 50%, and 75%. The heating rate was still selected to be 10 °C/min, with an average limestone size of 0.44 mm. The pyrolysis characteristic curves of small-particle limestone in a total of five reaction atmospheres of 0% CO₂, 25% CO₂, 50% CO₂, 75% CO₂, and 100% CO₂ are shown in Figure 4.

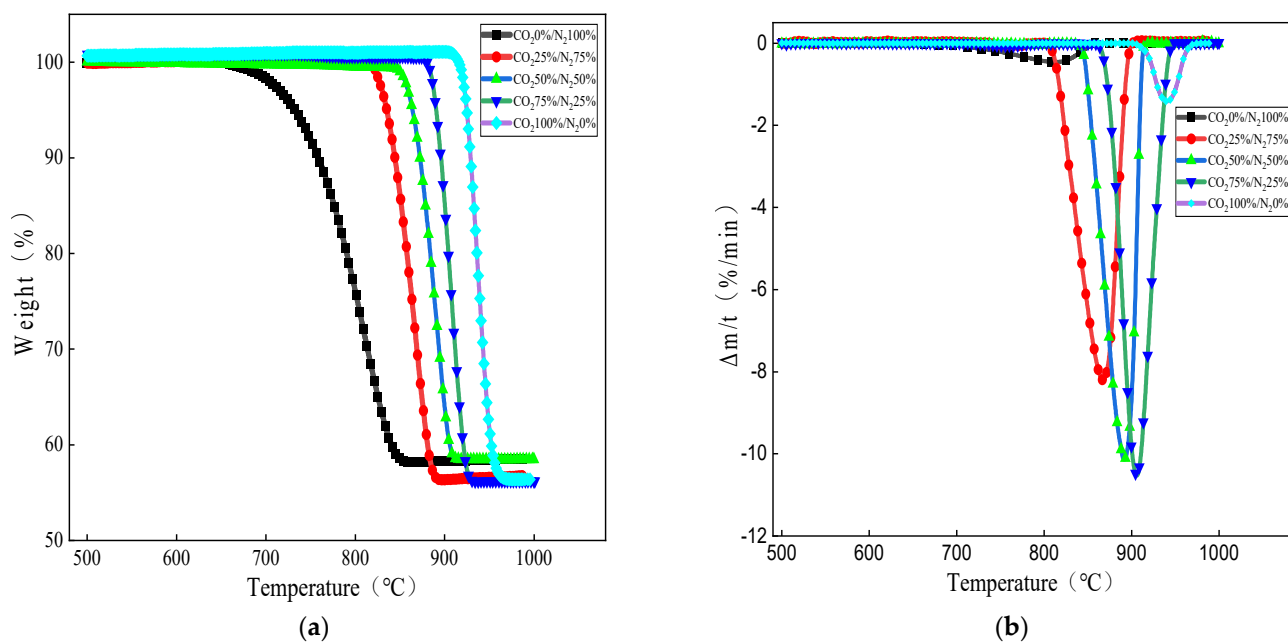


Figure 4. Effect of CO₂ partial pressures on limestone decomposition: (a) weight loss versus temperature curves at different partial pressures and (b) DTG curves of limestone decomposition under different partial pressures.

As can be seen from Figure 4a, under the five atmospheres shown, the limestone decomposition onset temperature is between 643 °C and 903 °C, and with the increase in CO₂ partial pressure, the limestone decomposition onset and completion temperatures produce a hysteresis. As the CO₂ concentration in the reaction atmosphere increases, the decomposition curve shifts to the higher temperature region. According to the Le Chatelier principle, when the partial pressure of CO₂ in the atmosphere is lower than the equilibrium partial pressure, calcium carbonate decomposes in the forward direction; conversely, the reaction reverses to produce calcium carbonate. Therefore, the decomposition reaction is controlled by the partial pressure of CO₂ and the reaction temperature. The limestone produces part of CO₂ during decomposition, and as the partial pressure of CO₂ increases, limestone decomposition is inhibited, and the process of CO₂ escape is greatly inhibited, resulting in a lag in decomposition temperature. In a high concentration CO₂ atmosphere, calcium carbonate can decompose, because in non-constant temperature and pressure conditions, the calcium carbonate decomposition temperature of CO₂ is much higher than the temperature of the carrier gas, so it can be desorbed into solids to escape, ensuring that the decomposition of calcium carbonate can continue. In addition, as can be seen from Figure 4b, with an increase in CO₂ partial pressure, the peak temperature of limestone decomposition also corresponds to the hysteresis. As the CO₂ partial pressure progressed

from 0 to 50%, the limestone decomposition reaction rate growth is very large, the peak is steeper, and the peak reaction rate increases; as the CO₂ partial pressure progresses from 50% to 75%, the growth of the limestone decomposition reaction rate is greatly reduced compared to the lower concentrations and the peak reaction rate increases slightly. Combined with Figure 3a,b, this indicates that the CO₂ partial pressure does produce a certain inhibition on the decomposition of limestone, although the inhibition is not obvious when the CO₂ partial pressure is lower. There is a limited link between CO₂ partial pressure and the decomposition rate of limestone, and the inhibition is more significant at high CO₂ partial pressure, but the reactions are all completed by 1000 °C.

3.4. Effect of CO₂ Partial Pressure on the Thermal Decomposition Kinetics of Small-Particle Limestone

Based on the study of CO₂ partial pressure on the thermal decomposition behavior of limestone in Section 2.3, in order to further calculate the kinetic parameters and kinetic model for the rapid thermal decomposition of small-particle limestone at the temperature of converter steelmaking, the atmospheric partial pressures of 0%, 25%, 50%, 75%, and 100% CO₂ and heating rates of 20 °C/min, 30 °C/min, and 40 °C/min were used. The average limestone particle size was 0.44 mm. In this subsection, the improved double extrapolation method is used to calculate the conversion rate of limestone using the TG-DTG curve obtained from the thermal decomposition of limestone to solve the activation energy of limestone thermally decomposed under different partial pressures of carbon dioxide. Furthermore, the temperature increase rate is extrapolated to zero to obtain the activation energy of limestone in thermal equilibrium. The apparent activation energy of limestone in the initial state clarifies the most generalized mechanism model of the limestone decomposition reaction, taking 25% CO₂ as an example. The following Figure 5 shows the curve of the thermal decomposition of limestone under different heating rates when the CO₂ partial pressure is 25%.

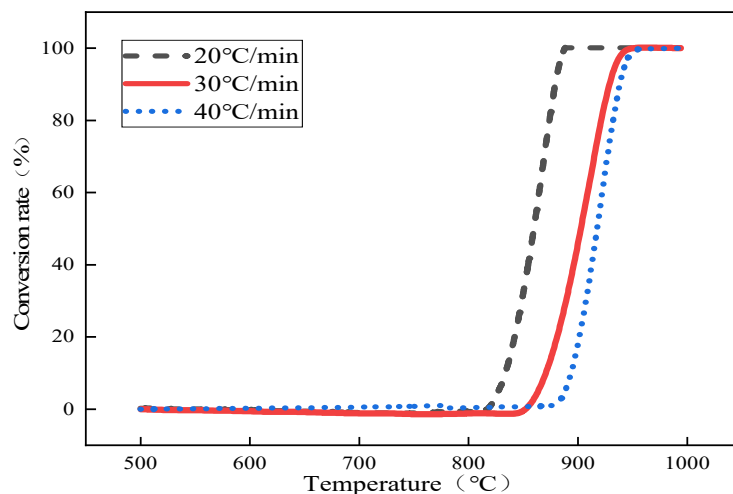


Figure 5. Conversion rate versus temperature curve at 25% CO₂ partial pressure.

According to the conversion rate curve of limestone, the temperatures corresponding to the conversion rate of limestone at different heating rates under 25% CO₂ partial pressure were obtained, as shown in Table 4 below.

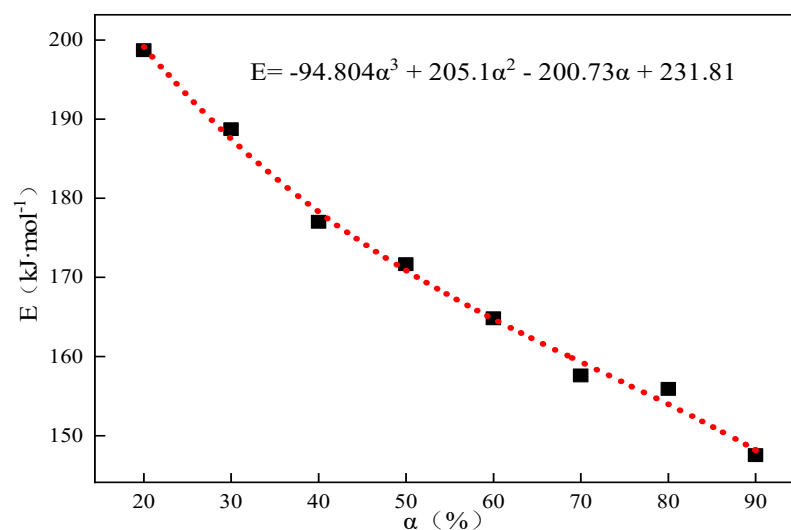
By utilizing the same research method as in Section 2.1, the conversion rate was fixed, and the corresponding activation energies, E , at different conversion rates were found according to the Starink differential equation, $\ln(\beta/T^{1.8}) = C_s - 1.0037E/RT$, and $E = \alpha_1 + b_1\alpha + c_1\alpha^2 + d_1\alpha^3$. The corresponding activation energies at different conversion rates were obtained and fitted to obtain $E_{\alpha \rightarrow 0} = 231.81 \text{ kJ}\cdot\text{mol}^{-1}$ without any interference of the side reactions when the system was in the pristine state, and the results are shown in Table 5 and Figure 6, respectively.

Table 4. Reaction temperatures for each conversion at different heating rates.

Conversion Rate (%)	Temperature/°C (20 °C/min)	Temperature/°C (30 °C/min)	Temperature/°C (40 °C/min)
20	832.07	852.91	865.33
30	841.74	862.12	877.46
40	849.45	873.19	887.74
50	857.65	882.62	897.57
60	867.56	888.85	910.15
70	873.15	899.02	917.94
80	878.95	907.32	924.15
90	886.21	916.87	934.31

Table 5. Corresponding linear fitting equations at different conversion rates in 25% CO₂.

Conversion Rate (%)	Linear Fitting Equation	Fitting Factor (R ²)	E (kJ·mol ⁻¹)
20	$\ln(\beta/T^{1.8}) = -23984\frac{1}{T} + 12.074$	0.9965	198.68
30	$\ln(\beta/T^{1.8}) = -22782\frac{1}{T} + 10.797$	0.9993	188.72
40	$\ln(\beta/T^{1.8}) = -21369\frac{1}{T} + 9.3819$	0.9972	177.02
50	$\ln(\beta/T^{1.8}) = -20723\frac{1}{T} + 8.6581$	0.9964	171.67
60	$\ln(\beta/T^{1.8}) = -219897\frac{1}{T} + 7.7847$	0.9956	164.82
70	$\ln(\beta/T^{1.8}) = -19023\frac{1}{T} + 6.9108$	1	157.58
80	$\ln(\beta/T^{1.8}) = -18822\frac{1}{T} + 6.6348$	0.9947	155.92
90	$\ln(\beta/T^{1.8}) = -17808\frac{1}{T} + 5.6463$	0.9941	147.52

**Figure 6.** Thermal decomposition of limestone at 25% CO₂ partial pressure corresponding to the E- α relationship curve.

The same method was used to obtain the results of the limestone activation energy changes at partial pressures of 0%, 25%, 50%, 75%, and 100% CO₂, and the activation energy data obtained were fitted and extrapolated to obtain the activation energy of the limestone in its original state, as shown in Table 6.

Based on Table 5, the apparent activation energy E was obtained by fixing the heating rate β , substituting the Coats–Redfern integral equation, and then extrapolating β to zero to obtain the value of $E_{\beta \rightarrow 0}$ at thermal equilibrium under the partial pressure of 25% CO₂. The following Table 7 shows a few kinetic parameters with good fits in the 47 reaction mechanism functions corresponding to $E_{\beta \rightarrow 0}$ and R².

Table 6. Activation energies corresponding to limestone in its pristine state at different CO₂ partial pressures.

Partial Pressure of CO ₂	E _{α→0} (kJ·mol ⁻¹)
0	201.9
25%	231.81
50%	250.32
75%	310.42
100%	347.11

Table 7. Apparent activation energies and correlation coefficients corresponding to mechanism functions with good linearity at different warming rates.

G(α)	0 °C/min		20 °C/min	
	E _{β→0} (kJ·mol ⁻¹)	R ²	E (kJ·mol ⁻¹)	R ²
α + (1 - α) ln(1 - α)	911.78	1	638.39	0.9888
[1 - (1 - α) ^{1/3}] ²	1047.6	1	744.56	0.9946
(1 - 2α/3) - (1 - α) ^{2/3}	956.45	0.996	673.22	0.9916
1 - (1 - α) ^{1/2}	477.68	0.999	336.79	0.9923
1 - (1 - α) ^{1/3}	515.08	0.999	362.87	0.9943
-ln(1 - α)	588.44	1	420.69	0.9937
[-ln(1 - α)] ^{2/3}	386.47	1	274.19	0.9934
[-ln(1 - α)] ^{1/2}	285.49	0.998	200.94	0.9931
[-ln(1 - α)] ^{1/3}	184.51	0.997	127.69	0.9924
[-ln(1 - α)] ^{2/5}	228.92	1	156.99	0.9928
[-ln(1 - α)] ^{1/4}	134.02	0.999	91.06	0.9917
[-ln(1 - α)] ^{3/4}	436.99	1	310.82	0.9935
G(α)	30 °C/min		40 °C/min	
	E (kJ·mol ⁻¹)	R ²	E (kJ·mol ⁻¹)	R ²
α + (1 - α) ln(1 - α)	565.93	0.9813	536.31	0.989
[1 - (1 - α) ^{1/3}] ²	662.24	0.9926	626.06	0.9947
(1 - 2α/3) - (1 - α) ^{2/3}	597.51	0.9861	565.75	0.9918
1 - (1 - α) ^{1/2}	298.34	0.9875	281.23	0.9924
1 - (1 - α) ^{1/3}	321.49	0.9921	303.28	0.9943
-ln(1 - α)	374.03	0.9967	352.16	0.9936
[-ln(1 - α)] ^{2/3}	242.94	0.9965	228.27	0.9933
[-ln(1 - α)] ^{1/2}	177.39	0.9963	166.33	0.9929
[-ln(1 - α)] ^{1/3}	111.85	0.9958	104.39	0.992
[-ln(1 - α)] ^{2/5}	138.06	0.9961	129.17	0.9925
[-ln(1 - α)] ^{1/4}	79.07	0.9953	73.42	0.991
[-ln(1 - α)] ^{3/4}	275.71	0.9965	259.25	0.9934

According to the values of E_{β→0} obtained in Table 7 compared with the previously obtained E_{α→0} = 231.81 kJ·mol⁻¹, the value of E_{β→0} = 228.92 kJ·mol⁻¹ in Table 7 is the closest and the fit is high. Therefore, the corresponding model for the thermal decomposition of limestone at a partial pressure of 25% CO₂ is a random nucleation and subsequent growth model, and the number of reaction levels is 2/5. Similarly, the values of E_{β→0} of limestone extrapolated from the partial pressures of 0%, 25%, 50%, 75%, and 100% CO₂ are summarized as shown in Table 8.

Table 8. Activation energies and mechanism functions corresponding to the thermal decomposition of limestone at different CO₂ partial pressures.

Partial Pressure of CO ₂	E _{β→0} (kJ·mol ⁻¹)	R ²	G(α)	n
0	204.99	0.999	$[-\ln(1-\alpha)]^{2/3}$	2/3
25	228.92	1	$[-\ln(1-\alpha)]^{2/5}$	2/5
50	249.48	0.998	$[-\ln(1-\alpha)]^{2/5}$	2/5
75	309.03	0.999	$[-\ln(1-\alpha)]^{1/2}$	$\frac{1}{2}$
100	340.2	1	$[-\ln(1-\alpha)]^{1/2}$	$\frac{1}{2}$

Comparing the mechanism function of the thermal decomposition of limestone under different CO₂ partial pressures in high temperature and rapid calcination, the reaction models are stochastic nucleation and subsequent growth models. Limestone decomposition initially occurs in some localized areas, and then as the reaction proceeds, these adjacent decomposition products will be aggregated to form a new phase, CaO; then, the surrounding CaCO₃ molecules continue to undergo the interfacial reaction until the entire solid phase is completely decomposed. The functional equation of the mechanism is $G(\alpha) = [-\ln(1-\alpha)]^n$, and the CO₂ partial pressure is different when the number of levels of the reaction changes; As the CO₂ partial pressure of 25% increased to 100%, the activation energy of thermal decomposition gradually increased, and the number of reaction levels, n, increased.

4. Conclusions

- (1) With the increase in heating rate, the decomposition temperature of small particles of limestone increases. The apparent activation energies of the decomposition of limestone with average particle sizes of 0.44 mm and 2.5 mm is 250.32 kJ·mol⁻¹ and 328.27 kJ·mol⁻¹, respectively, and with the increase in limestone particle size, the apparent activation energy of the thermal decomposition of limestone increases, and the difficulty of the decomposition reaction increases.
- (2) Compared with N₂, air, and O₂ atmospheres, in the pure CO₂ atmosphere, limestone thermal decomposition reaction completion temperature increases, but the time required for decomposition is shortened. With the increase in the partial pressure of carbon dioxide, limestone decomposition is inhibited and the decomposition temperature lags. However, the decomposition reaction occurs more intensely as the limestone decomposition speed is accelerated, and time required to complete the decomposition is shortened.
- (3) At low CO₂ partial pressures, the limestone decomposition temperature produces a hysteresis as the partial pressure increases and the reaction rate increases by a large amount. Under high CO₂ partial pressure, the inhibition is more significant, and the reaction rate slows down, but the reaction can be fully reacted within 1000 °C.
- (4) The thermal decomposition reactions of small-grained limestone at different CO₂ partial pressures at steelmaking temperatures are all consistent with the model of both stochastic nucleation and subsequent growth, and the functional equation of the mechanism is $G(\alpha) = [-\ln(1-\alpha)]^n$; the activation energy of the decomposition reaction gradually increases when the CO₂ partial pressure is increased from 25% to 100%, the number of reaction stages n increases, and the difficulty of the reaction increases.

However, subsequent studies on the reaction mechanism of small-grained limestone at steelmaking temperatures, especially those related to the decomposition behavior of small-grained limestone under different CO₂ partial pressures, will continue. Also, the subject of the slagging of converter-blasted small limestone will continue to be fully investigated under the prerequisites of ensuring proper blowing size, atmosphere conditions, and optimum parameters for phosphorus removal. This will be demonstrated by thermodynamic calculations and thermal experiments in our subsequent work.

Author Contributions: C.L. and Y.X. conceived and designed the study; Y.Z. and H.S. performed the calculations; Y.Z. conducted the experiment; K.Z., H.X. and S.W. analyzed the experimental data; and C.L. and Y.Z. wrote the paper. All authors have read and agreed to the published version of the manuscript.

Funding: This research was funded by the National Natural Science Foundation of China, grant number 52274334 and 52004097, and the Science and Technology Research Program for Higher Education Institutions in Hebei Province, grant number BJK2022059.

Data Availability Statement: Not applicable.

Acknowledgments: Thanks to X. Meng and H. Shen of North China University of Science and Technology for checking and revising the manuscript.

Conflicts of Interest: The authors declare no conflict of interest.

References

1. Zhang, Q.; Shen, J.-L.; XU, L.-S. Carbon peak and low-carbon transition path of China's iron and steel industry. *Iron Steel* **2021**, *56*, 152–163.
2. Cui, Z.-F.; Xu, A.-J.; Shangguan, F.-Q. Low-carbon development strategy analysis of the domestic and foreign steel industry. *Chin. J. Eng.* **2022**, *44*, 1496–1506.
3. Zhang, F.-M.; Liu, Q.-M. Development and understanding on low carbon technology based on BF-BOF steel manufacturing processes. *China Metall.* **2023**, *33*, 1–17.
4. Somnath, B.; Ashok, K.L.; Seshadri, S.; Halder, J. Change in phosphorus partition during blowing in a commercial BOF. *ISIJ Int.* **2007**, *47*, 766.
5. Ye, G.-F.; Yang, J.; Lu, X.-W.; Wang, H.; Liu, W.-S.; Zhang, R.-H.; Yang, W.-K. Effects of operation parameters on dephosphorization results of BOF at low temperature and low basicity. *Steelmaking* **2019**, *35*, 16–23.
6. Zhang, R.-H.; Yang, J.; Ye, G.-F.; Sun, H.; Yang, W.-K. Latest development of dephosphorization process in converter steelmaking. *Steelmaking* **2022**, *38*, 1–13.
7. Zeng, J.-Q.; Yang, L.-B.; Wang, J.; Liu, X.-L.; Yao, T.-L.; Dai, S.-F. Effect of bottom blowing on dephosphorization technology in combined blowing converter. *Iron Steel* **2017**, *52*, 40–44+51.
8. Zhi, J.-G.; Wu, W.; Gao, Q.; Xu, T.; Luo, H.-M.; Zhang, X.-F. Effect of improving dephosphorization of molten steel by optimizing slagging in large converters. *Iron Steel* **2020**, *55*, 72–77.
9. Chen, L.; Diao, J.; Wang, G.; Xie, B. Assessment of dephosphorization during vanadium extraction process in converter. *JOM* **2018**, *70*, 46–51. [[CrossRef](#)]
10. Li, H.; Qu, Y. Discussion on limestone addition instead of lime for energy-saving and emission reduction in BOF steelmaking. *China Metall.* **2010**, *20*, 45–48.
11. Katherine, L.; Yang, Y.D.; Mansoor, B.; McLean, A. Dephosphorization of levitated silicon-iron droplets for production of Solar-Grade Silicon. *Metall. Mater. Trans. B* **2018**, *49*, 21–25.
12. Diao, J.; Shao, L.; Liu, D.; Qiao, Y.; Tan, W.; Wu, L.; Xie, B. Removal of Phosphorus from Leach Liquor of Steel Slag: Adsorption Dephosphorization with Activated Alumina. *JOM* **2018**, *70*, 36–40. [[CrossRef](#)]
13. Davide, M.; Carlo, M.; Silvia, B.; Gruttadauria, A.; Sosio, R.; Valentino, G.; Ancona, V. Model for phosphorus removal in LD converter and design of a valuable operative practice. *Steel Res. Int.* **2018**, *89*, 46–51.
14. Mao, W.-W.; Li, C.-X.; Lu, H.; Hu, L.-F.; Li, H.; Cao, Z.-M. Silicon volatilization in the form of SiO during slagging by limestone in BOF. *Ironmak. Steelmak.* **2017**, *44*, 389–393. [[CrossRef](#)]
15. Mao, W.; Li, C.; Lu, H.; Li, H.; Xie, W. Limestone dissolution and decomposition in steelmaking slag. *Ironmak. Steelmak.* **2018**, *45*, 720–726. [[CrossRef](#)]
16. Lu, H.; Li, C.-X.; Mao, W.-W.; Li, H. Laboratory study of CaCO₃ decomposition, influence of BOF converter slag. *Metall. Res. Technol.* **2017**, *114*, 20–26. [[CrossRef](#)]
17. Dong, K.; Wang, X.-L. CO₂ utilization in the ironmaking and steelmaking process. *Metals* **2019**, *9*, 273. [[CrossRef](#)]
18. Yi, C.; Zhu, R.; Chen, B.-Y.; Yi, C.; Zhu, R.; Chen, B.-Y.; Wang, C.-R.; Ke, J.-X. Experimental research on reducing the dust of BOF in CO₂ and O₂ mixed blowing steelmaking process. *ISIJ Int.* **2009**, *49*, 1694–1699. [[CrossRef](#)]
19. Lv, M.; Zhu, R.; Wei, X.; Wang, H.; Bi, X. Research on top and bottom mixed blowing CO₂ in converter steelmaking process. *Steel Res. Int.* **2012**, *83*, 11–15. [[CrossRef](#)]
20. Deng, T.; Patrice, N.; Ek, M.; Du, S. Limestone dissolution in converter slag at 1873 K (1600 °C). *Metall. Mater. Trans. B* **2013**, *44*, 98. [[CrossRef](#)]
21. Lu, W.-G.; Zhu, R.; Yu, H. Research on slagging by limestone during BOF steelmaking process. *Chin. J. Eng.* **2016**, *38*, 78–82.
22. Liang, Y.-C.; Tang, H.-Y.; Li, J.-S.; Guo, S.-L.; Wang, G.-F.; Dan, J.-Q.; Yang, H.-B.; Li, H. Laboratory study on dephosphorization with limestone substituting for some lime. *J. Chongqing Univ.* **2015**, *38*, 83–88.
23. Tang, B.; Wang, X.-M.; Zou, Z.-S.; Sun, G.-Q. Physical simulation of BOF limestone particles blowing via top lance. *J. Northeast. Univ. (Nat. Sci.)* **2014**, *35*, 695–699.

24. Zhang, B.; Wu, W.; Wu, W.; Wang, T.-M.; Luo, L.-G.; Wang, Y.-H. Water model of freely swing lance injecting limestone powder to dephosphorization. *Iron Steel* **2019**, *54*, 28–32.
25. Wang, L.-Y.; Xue, Z.-L.; Chen, K.-F.; Hu, B. High-temperature decomposition kinetics of large particle-size limestone. *J. Chongqing Univ.* **2020**, *43*, 32–46.
26. Cao, J.; Qiao, X.-C.; Liu, C.-L.; Zhang, J.-S. A study on kinetics of limestone decomposition in air and CO₂ atmospheres. *Inorg. Chem. Ind.* **2016**, *48*, 32–36.
27. Zhang, W.-X.; Liu, L.-S.; Cao, H.-J.; Wu, B.-K.; Cheng, Z.-P. Effect on kinetics of limestone decomposition under different CO₂ atmospheres. *Inorganic Chem. Ind.* **2020**, *52*, 59–63.
28. Chen, H.; Zhang, S.-H.; Yang, H.-P.; Li, P.; Chen, H.-P.; Zeng, J. Study on thermal decomposition kinetics of limestone with large particle size. *Inorg. Chem. Ind.* **2013**, *45*, 11–14. [[CrossRef](#)]
29. Li, C.-X.; Li, H.; Zhou, B.; Lv, Y.-C.; Qin, D.-P.; Wei, S.-H. Experimental study on steelmaking using limestone instead of lime as the slagging material in 100t converter. *China Metall.* **2015**, *25*, 22–26+49.
30. Lu, H.; Li, C.-X.; Mao, W.-W.; Li, H. The effect of CO₂ oxidation on hot metal arising from CaCO₃ decomposition in BOF. *Steelmaking* **2017**, *33*, 49–55.
31. Sun, H.-K.; Li, C.-X.; Wang, S.-H.; Zhang, K.-X.; Tong, S.; Zhang, Y. Research on microstructure evolution behavior of small particle limestone during rapid calcination at high temperature. *Steelmaking* **2022**, *38*, 38–42+58.
32. Hu, R.-Z.; Gao, S.-L.; Zhao, F.-Q. *Thermal Analysis Kinetics*; Beijing Science Press: Beijing China, 2008; pp. 29–30, 119–120, 138–140, 151–155.

Disclaimer/Publisher’s Note: The statements, opinions and data contained in all publications are solely those of the individual author(s) and contributor(s) and not of MDPI and/or the editor(s). MDPI and/or the editor(s) disclaim responsibility for any injury to people or property resulting from any ideas, methods, instructions or products referred to in the content.